THIRTEENTH EUROPEAN ROTORCRAFT FORUM

2.18

Paper No. 94

RESULTS FROM THE GLASGOW UNIVERSITY BLADE/VORTEX INTERACTION (B.V.I.) FACILITY

A. KOKKALIS

R.A.McD. GALBRAITH

UNIVERSITY OF GLASGOW
U.K.

September 8 - 11, 1987

ARLES, FRANCE

RESULTS FROM THE GLASGOW UNIVERSITY BLADE/VORTEX INTERACTION (B.V.I.) FACILITY

SUMMARY

A wind tunnel test program using an instrumented model rotor blade has been conducted to determine both representative and critical blade/vortex interaction (B.V.I.) airloads. In particular, the parallel B.V.I. case was investigated in detail; instantaneous blade airloads were measured for a variety of vortex strengths and blade/vortex separation distances at two spanwise locations. The data revealed that the basic effect of the vortex interactions was a rapid continuous pressure pulse, predominately manifesting itself over the forward 25% of the airfoil. Comparisons of the measured Normal force coefficient history with that predicted by the method of Beddoes show good agreement, both in magnitude and shape.

NOMENCLATURE

C	Rotor blade chord
C_W	Vortex generator airfoil chord
C_N	Normal force coefficient ($\int_0^x C_p dx$)
$C_{M\frac{1}{4}}$	¼-Chord pitching moment coefficient
C_p	Pressure coefficient (= $(P-P_o)/\frac{1}{2}\rho U_T^2$)
$C_{P0.05}$	Pressure coefficient at x/C = 0.050, along the upper surface of the airfoil.
C_T	Pressure drag coefficient (=$\int_0^y C_p dy$)
d_v	Vortex core diameter
M_L	Mach number at the position of measurements
P	Local dynamic surface pressure at ($U_T + U_o$)
P_o	Local surface pressure at velocity U_T
r	Position along the rotor blade span
R	Rotor blade span
U_o	Free stream flow velocity
U_T	Rotational speed of blade-tip
x	Position along the rotor blade chord from leading edge
X_v	Distance of vortex from leading edge of airfoil (See Fig. 1)
y	Distance across the vortex centre (See Fig. 4)
Y_v	Distance of vortex, from airfoil chord (See Fig. 1)
Γ	Vortex strength
δ	Differential angle-of-attack of vortex generator
ρ	Density of air
ψ	Angle of rotation along the azimuth

INTRODUCTION

In most flight conditions, the tip vortices shed by the rotor blades of a helicopter tend to pass under its effective rotor disc. This is not so, however, for flight conditions such as steady descent, where the resulting net positive inflow tends to force the wake into the rotor disc plane. In consequence of this, strong blade-vortex interactions occur (Fig. 1). Such interactions induce significant changes in the blade circulation and hence

variations in the blade's airloading. It has been established, both by experiment and theory (1) that the severity of the interaction, i.e. the magnitude and rate-of-change of the blades airloading, is strongly related to the following:

(a) Strength and core size of the interacting vortex
(b) Local interaction angle between the blade and the tip vortex
(c) Vertical separation between the vortex and the blade

Over the past two decades, research has been conducted to assess and understand the details of the Blade-Vortex Interactions (B.V.I.'s) (3,7,8). The incentive for the work stems from B.V.I. being identified as a major contributor to helicopter fuselage vibrations and radiated aerodynamic noise (2,3). The satisfactory prediction of such loadings at an early stage of rotor blade design is, therefore, advantageous.

Currently, a number of computational techniques are used for the assessment of B.V.I. induced airloads (4,5,6), but it has been difficult to assess their predictive capabilities. A major cause of this, is the dearth of experimental data on B.V.I.'s and, also, the difficulty of investigating such phenomena on a full scale rotor during flight. Much can be learned, however, by the study of B.V.I. in the controlled environment of a wind tunnel and such techniques have been used successfully in previous B.V.I. investigations (7,8). Such a facility has been commissioned at the University of Glasgow and this paper presents selected data from it and discusses comparisons between the measured Normal force coefficient and that predicted by the theoretical model of Beddoes (4).

DESCRIPTION OF TEST FACILITY

The facility was constructed in the 2.1 x 1.6 m "Handley-Page" low speed wind tunnel at the University of Glasgow. The phenomenon of B.V.I. was modelled by means of a rotating blade interacting with a vortex, generated from an upstream stationary airfoil. A diagram of the test ring is shown in Fig. 2 and a full description has been presented in Ref. 9.

The interacting vortex was generated at the juncture of two adjacent wings mounted vertically from floor-to-ceiling and located 8.1 chordlengths upstream of the rotor tip whilst at an azimuth of $\Psi = 180^{\circ}$. The wings had a 0.15m chord (Cw) with a constant NACA 0015 profile. The vortex strength (Γ), was varied by setting the wings at equal but opposite angles-of-attack. Also, the vertical position of the vortex was adjusted via a re-alignment of small blade elements at the wing juncture. To locate the vortex trajectory and assess its characteristics, both smoke flow visualisation and hot-wire measurements (using a 3-wire probe) were carried-out. Hot wire data were recorded at several vertical positions over a distance of 0.12m (0.8Cw) either side of the perceived vortex centre and along the horizontal plane of symmetry.

The rotor consisted of a single untwisted blade of NACA 0015 profile with a chord (C) of 0.15m and an aspect ratio of 5.10. The blade was numerically machined from Duraluminium and had first flap and torsional frequencies of 27Hz and 163Hz respectively. The outer 50% of the blade's span was so designed as to incorporate an instrumentation pod containing 23 pressure

transducers (ENTRAN, type EPIL-80-55). This pod was interchangeable with other modules to permit the positioning of the transducers at any of the spanwise positions r/R 0.55, 0.65, 0.75, 0.85 and 0.95.* The chordal distribution of the pressure transducers is given in Table 1.

The transducer signals were amplified and filtered before being digitised using a transient digital recorder (Thorn-EMI, type BE256-420). At the completion of a run, the digitised signals were transfered, via an IEEE-488 bus, to a MINC (PDP 11/23+) microcomputer for preliminary evaluation and storage. Final analysis of the recorded data was carried out using a VAX 11/750, at which stage data were ensemble-averaged to reduce random flow and electrical noise effects. This averaging was for the five data records of 300 samples/channel taken over the appropriate 140^0 sector in each rotor revolution.

RESULTS

Data was acquired over a range of vortex strengths, blade-vortex separation distances, and for two spanwise locations. A summary of these tests is given in Table 2. The results presented in this paper, however, are only for tests in which the vortex generator was set at a differential angle-of-incidence (δ) of 25^0 and the pressure transducers located at the spanwise position r/R = 0.95. For the present discussion, therefore, the only variable to consider is the relative location of the vortex to the blade (i.e., Y_V/C).

A typical variation of the non-dimensionalised tangential velocity (U_T/U_o) profile across the core of the vortex for a generator differential angle-of-incidence of $\delta = 25^0$, is shown in Fig. 3. It may be seen that the structure of the vortex is fairly well defined and the viscous core region (taken as the distance to the maximum tangential velocity) is about 0.04m (or 0.27 Cw) in diameter. Figure 4 presents both the vortex strength and core diameter for all six differential angles investigated. The vortex strengths were calculated by assuming axial symmetry and the velocity profile being represented by Scully's method (10). As can be seen, the vortex strength is not a simple linear function of the differential incidence, and the core radius decreases as the differential incidence increases.

The set of pressure histories on the vortex side (upper surface) of the blade when the blade-to-vortex separation distance was $Y_v/C = 0.20$, are shown in Fig. 5. For these illustrations they have been plotted on a scale of a chord-transit interval, ranging from 1.35C upstream of the leading edge to 1.55C downstream the trailing edge. By far the most important event observed, is the occurance of a sharp pressure perturbation as the vortex approaches and passes the leading edge. The associated timing of the very abrupt pressure rise is of the order of 0.55 chord lengths of travel. It may be seen that the pressure rise at the first transducer (i.e., x/C = 0.015) occurs at about 0.10C, in time, ahead of that at the

---

* To date, measurements have been taken at the spanwise locations of r/R = 0.75 and r/R = 0.95.

second position (x/C = 0.030). However, the pressure rise at the second transducer and all those up to x/C = 0.10, occur at effectively the same time. This is followed by a more gentle pressure rise at between x/C = 0.15 and x/C = 0.35, with the speed of pressure wave propagation being greater than the speed of vortex travel. The interpretation of the pressure variation is complicated at the position of x/C = 0.35 by the appearance of a compression type pulse at X_v/C = 0.10. For chordwise positions greater than x/C = 0.35, it may be observed, that the magnitude of the compression pulse increases while its speed of propagation decreases. At x/C = 0.76, the pressure variation has changed from the characteristic type mentioned above, to that of compression travelling with the speed of vortex. The varying nature and speed of propagation of the pressure pulse clearly shows the complexity of the flow near the surface of the airfoil, during the vortex-boundary layer interaction.

A set of upper surface (vortex side) pressure variatons for a much weaker B.V.I. case (Y_v/C = 0.60) is shown in Fig. 6. Although the general trends of the pressure histories are similar to those observed in the stronger B.V.I. case (Y_v/C = 0.20), there exist several important differences between the two. At the leading edge the pressure rise is more gradual than for Y_v/C = 0.20. Also, the delay time of the pressure rise between the position of the first transducer and that of the second is greater; being 0.30C. However, the most striking differences occur at chordwise positions greater than x/C = 0.20 where there exists no evidence of a change in either the speed of travel, or nature of the pressure pulse discussed above.

Since the only difference between these two cases is the blade/vortex separation distance, it may be concluded that the observed variations in both the nature and propagation speed of the pressure pulse at Y_v/C = 0.20 are due to the manner which tip vortices interact with the boundary layer of the blade. This conclusion is further supported by Fig. 7 where the pressure variations at x/C = 0.050 for Y_v/C = 0.00, 0.20, 0.40, 0.60 and 0.80 are presented. Although the qualitative nature of the pressure variation is similar for all cases shown, the magnitude of the pressure pulse is seen to rise rapidly with decreasing Y_v/C values. Such trends indicate that vortex induction effects upon the blade rapidly increases as the blade/vortex separation distance decreases.

The lower surface pressure variations corresponding to the above strong and weak B.V.I., are presented in Fig. 8 where it may be observed that the main features of both plots are similar. Also, the large pressure perturbations are concentrated at the forward 25% of the chord, and have the opposite sign of that observed on the upper surface. Furthermore, the magnitude of the pressure pulse is smaller and more gradual than on the vortex side. There is still, however, an observable delay between the pressure rise at the position of the first transducer and that of the second, this being 0.05C at Y_v/C = 0.20 and 0.20C at Y_v/C = 0.60. At x/C positions greater than 0.25, there are interesting differences between the pressure traces. For the strong B.V.I. case, a secondary pressure pulse appears at x/C = 0.35, the effect of which increases with distance downstream while its speed of travel decreases. For x/C locations greater than 0.55, only this type of pulse is evident, travelling with the approximate speed of vortex. This pressure pulse is similar to that observed on the vortex side of blade for Y_v/C = 0.20. No such trends were observed for the weak B.V.I. case.

The chordal variations of the pressure coefficient at selected X_v/C positions for $Y_v/C = 0.20$ are shown in Fig. 9. In Figs. 9a and 9b which represent the pressure distributions for the vortex at 1.52 and 0.96 chord-lengths ahead of the leading edge, the distributions resemble those associated with "static" behaviour at increasing incidence. In general, as the vortex approaches the leading edge, the suction pressure increases until it reaches its maximum at $X_v/C = -0.24$ (Fig. 9c). This location corresponds to that at which both the normal force and pressure drag coefficients attained their maximum and minimum values respectively and the ¼-chord pitching moment reached its minimum nose-down value (See Fig. 11). As the vortex moved closer to the airfoil, the leading edge suction pressure decreased while that over the rear part of the airfoil remained much the same with a small increase (Fig. 9d). This resulted in a decreased normal force coefficient, an increased pressure drag and a large nose-down ¼-chord pitching moment coefficient. As the vortex moves over the airfoil, the pressure distribution experiences significant changes, Fig. 9e. An interesting observation from this figure is, that the pressure distribution over the forward 20%-chord has reversed sign, and the lower surface pressure exceeds that on the upper surface. Over the remainder of the airfoil, the upper surface pressure still exceeds that on the lower surface, albeit a small difference. The net effect of such a distribution is a zero normal force coefficient, whilst the pressure drag attains its maximum value as does the nose-down ¼-chord pitching moment coefficient. Further movement of the vortex across the airfoil enhances the pressure reversal, which reaches a maximum at $X_v/C = 0.80$ as illustrated in Fig. 9f. Here the normal force attains its lowest value (See Fig. 11a) and the ¼-chord pitching moment, its minimum nose-down value. Finally, when the vortex has passed the trailing edge (Figs. 9g and 9h), the resulting pressure distributions yield little change to the ¼-chord pitching moment coefficient while both the normal force and pressure drag coefficients continue to increase (Fig. 11).

The chordwise pressure coefficient variation for selected X_v/C locations at $Y_v/C = 0.60$ are shown in Fig. 10. These are similar to those of the previous B.V.I. case (i.e., for $Y_v/C = 0.20$) albeit, as may be seen in Fig. 12 the changes are more gradual. Perhaps the only major variation of interest is that the maximum positive differential pressure was attained much earlier, at $X_v/C = -0.96$, whilst the maximum negative differential pressure was reached at a later X_v/C position (i.e., $X_v/C = 1.06$) than those observed for the stronger B.V.I. case. Thus the apparent effect of the vertical blade-vortex separation distance Y_v upon the chordwise pressure distribution is primarily seen to be similar for both Y_v/C cases examined, albeit the closer the vortex to the airfoil, the greater the induced airloading was.

The integrated aerodynamic coefficients associated with these pressure distributions are presented in Fig. 11 and 12.* The general shape and trends of the C_N plots are in good agreement with those reported by Surendraiah (8) and Leverton (11). For the strong B.V.I. case (Fig. 11),

---

* the lettered annotations refer to the individual C_p plots of Figs. 9 and 10.

it may be seen that the very pronounced interaction gives a ΔC_N as high as 0.63, occuring over a time interval of about 1.1 chord-lengths. For the weak interaction (Fig. 12), however, it is a more gentle affair with a ΔC_N of 0.48 over a time interval of about 2-chord lengths. Also it is of interest to note that while the maximum C_N value for $Y_v/C = 0.60$ occurs at approximately 0.70C ahead of that seen at $Y_v/C = 0.20$, the minimum C_N values appear at almost the same X_v/C position for both cases.

In addition, there is good correspondence between the C_N and C_T plots with regard to their overall shape. It may be seen from both C_T plots (Figs. 11b and 12b) that as the vortex approaches the leading edge, the pressure drag decreases reaching a minimum at the same Y_v/C location where C_N attains its maximum. As the vortex passess over the leading edge, the pressure drag varies to positive, attaining it positive maximum value at a X_v/C location slightly ahead of that at which C_N attains its minimum value.
Similar trends have been observed in flight measurements reported by Brotherhood and Riley (12). It is also of interest to note, that the negative nature of C_T, as the vortex approaches the leading edge, further demonstrates the importance of the suction pressure in the leading edge region.

In addition to the good correspondence of the C_N and C_T histories, a further consideration of the leading edge C_p histories (See Figs. 5 and 6) reveals a similar result as is illustrated in Fig. 13 for the two considered B.V.I. cases. Such observations have been reported by Brotherhood (13) and they may be useful because, if a consistent correlation relationship can be established between the C_p and C_N histories, the gains in both cost and reduced analysis time, for carrying out some aspects of B.V.I. tests, would be significant. Correlations between C_N and $C_{P0.05}$ are given in Fig. 14, and cover the vortex interaction from 1.35C ahead of the leading edge to 1.5C behind the trailing edge. Correlation coefficients of 0.991 and 0.996 were obtained for the strong and weak B.V.I. cases respectively. Whilst these results are very encouraging, they do not allow a definite linear correlation between C_p and C_N to be established. They do, however, indicate that a useful relationship between C_p at leading edge and C_N, may exist.

Finally, a major incentive for the work was the provision of data for code validation. Figure 15 presents comparisons between the experimental C_N values and those obtained from the predictive code of Beddoes (14) for the strong B.V.I. case and at the r/R spanwise locations of 0.75 and 0.95. It may be seen that both theoretical and experimental results are in good agreement.

The theoretical predictions of the general shape and the maximum and minimum C_N values, at both spanwise locations are most encouraging. The data does highlight differences between experiment and predictions and they may merit further investigations.

CONCLUDING REMARKS

A facility has been constructed for the study of parallel and oblique B.V.I.'s. The facility permits measurement of both upper and lower surface

pressure variations to be taken simultaneously along the azimuth, and for a variety of vortex strengths, blade/vortex separation distances and spanwise positions. Consideration of the measurements indicate that the most salient feature of a B.V.I. is a short duration pressure pulse, the maximum of which occurs when the vortex core is close to the blade's leading edge. The magnitude of the pulse was observed to increase rapidly with decreasing blade/vortex separation distance, and although it was observable over the entire chord it primarily affected the forward 25%.

To summarise the observations it can be said that, as the vortex approaches the leading edge, the pressure difference between the upper and lower surfaces of the blade increases due to the increased effective incidence induced by the vortex. This pressure difference attains its maximum when the vortex core is close to the leading edge and then rapidly collapses as the vortex passes it. With further movement over the airfoil chord, the pressure on the vortex side of the blade becomes less than that on the opposite side, and so the blade experiences a negative normal force and a large nose-down ¼-chord pitching moment value. When the vortex is over one chord-length away from the blade's trailing edge, its effects upon the airfoil are small and the blade once again experiences a positive normal force. Finally, comparisons between the predictions of Beddoes and the data from the present tests show good agreement with small differences.

ACKNOWLEDGEMENTS

The authors wish to express their thanks to Prof. Richards for his support and encouragement and to Mr T. Beddoes of Westland Helicopters for valuable discussions and providing the theoretical results. Also our thanks to Mr A. Jones and P. Wilby of the RAE for their continual support.

This work has been carried out with the support of the Procurement Executive, Ministry of Defence, under contract number MOD 2048/30.

REFERENCES

1. SCHULTZ, F.H., YU, Y.H., "Helicopter Impulsive Noise: Theoretical and Experimental Status". Recent Advances in Aeroacoustics, Eds. A. Krothapalli and C.S. Smith, Springer-Verlag, 1983.

2. HOOPER, W.E., "The Vibratory Airloading of Helicopter Rotors", 9th European Rotorcraft Forum, Stressa, Italy, Sept., 1983.

3. BOXWELL, D.A., SCHULTZ, F.H., "Full-scale Measurements of Blade-Vortex Interaction Noise", 36th Annual National Forum of the American Helicopter Society, Washington, D.C., May 1980.

4. BEDDOES, T. "A Near Wake Dynamic Model", A.H.S. Proceedings of National Specialists Meeting on Aerodynamics and Aeroacoustics, Arlington, Texas, U.S.A. Feb. 1987.

5. JONES, H., CARADONNA, F.X., "Full Potential Modelling of Blade-Vortex Interactions", 12th European Rotorcraft Forum, Garmisch-Partenkirchen, F.R.G., Sept., 1986.

6. SRINIVASAN, G.R., McCROSKEY, W.J., "Numerical Simulations of Unsteady Airfoil Vortex Interactions", Vertica, Vol. 11., No. 1/2, pp. 3-28, 1987.

7. CARADONNA, F.X., LAMB, G.H., TUNG, C., "An Experimental Study of the Parallel Blade-Vortex Interaction", 10th European Rotorcraft Forum, The Hague, Netherlands, Aug., 1984.

8. SURENDRAIAH, M., "An experimental study of Rotor Blade-Vortex Interaction, NASA Cr 1573, May 1970.

9. KOKKALIS, A., GALBRAITH, R.A.McD., "Description of, and Preliminary Results from, a new Blade-Vortex Interaction Test Facility", 12th European Rotorcraft Forum, Garmisch-Partenkirchen, F.R.G., Sept. 1986.

10. SCULLY, M.P., "Computations of Helicopter Rotor Wake Geometry and its Influence on Rotor Harmonic Load", ASRL TR-178-1, M.I.T., March, 1985.

11. LEVERTON, J.W., "Helicopter Noise-Blade Slap, Part I: Review and Theoretical Study", NASA TN D-1971, Oct, 1963.

12. BROTHERHOOD, P., RILEY, M.J., "Flight Experiments on Aerodynamic Features Affecting Helicopter Blade Design", Vertica, Vol. 2, pp. 27-42, 1978.

13. BROTHERHOOD, P., "An Appraisal of Rotor Blade-Tip Vortex Interaction and Wake Geometry from Flight Measurements", AGARD - CP-334, May, 1982.

14. BEDDOES, T., Private Communication, Westland Helicopters, Yeovil, U.K.

x/c at -			
r/R = 0.75		r/R = 0.95	
Upper Surface	Lower Surface	Upper Surface	Lower Surface
0.000	0.007	0.000	0.007
0.015	0.030	0.015	0.030
0.030	0.060	0.050	0.060
0.050	0.100	0.075	0.150
0.075	0.150	0.100	0.350
0.100	0.200	0.125	0.550
0.150	0.350	0.200	0.760
0.200	0.550	0.350	0.920
0.350	0.760	0.550	
0.550	0.920	0.760	
0.760		0.860	
0.860		0.950	
0.950			

FIG. 1. CHORDWISE PRESSURE TRANSDUCER LOCATIONS

SPANWISE LOCATIONS r/R = 0.75, 0,95							
Y_v/C / δ^o	-0.20	0.00	0.20	0.40	0.60	0.80	1.00
5.0	*	*	*	*	*	*	*
10.0	*	*	*	*	*	*	*
15.0	*	*	*	*	*	*	*
20.0	*	*	*	*	*	*	*
25.0	*	*	*	*	*	*	*

TABLE 2: SUMMARY OF TESTS

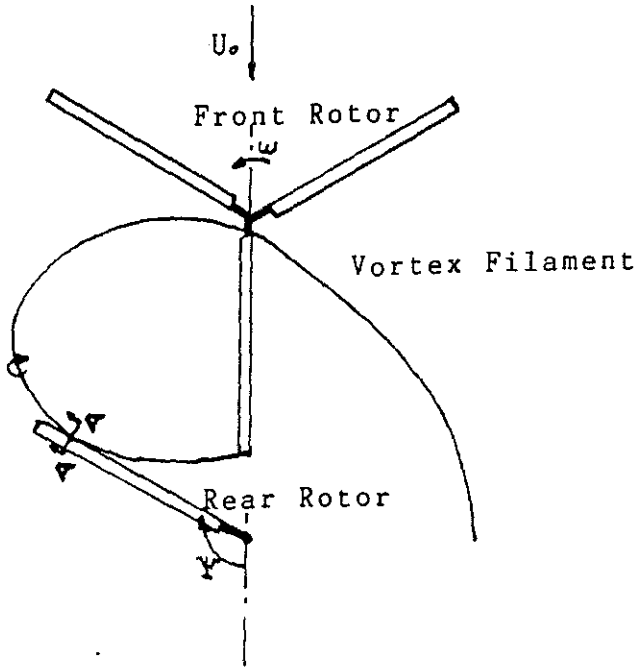

(a) Tandem Rotor

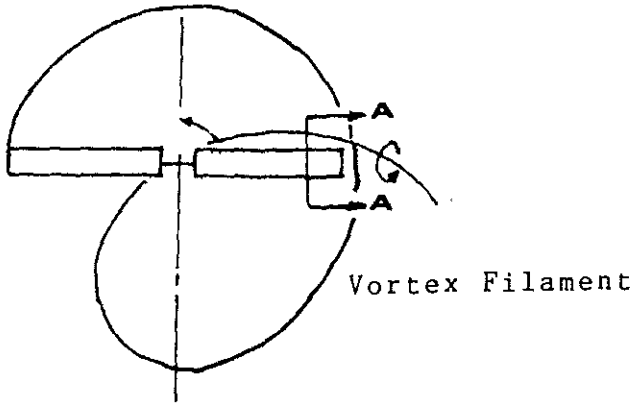

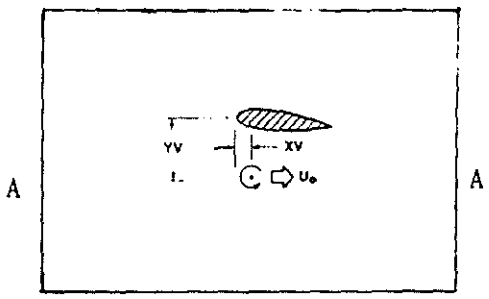

(b) Single Rotor

FIG. 1. PARALLEL BLADE VORTEX ENCOUNTER

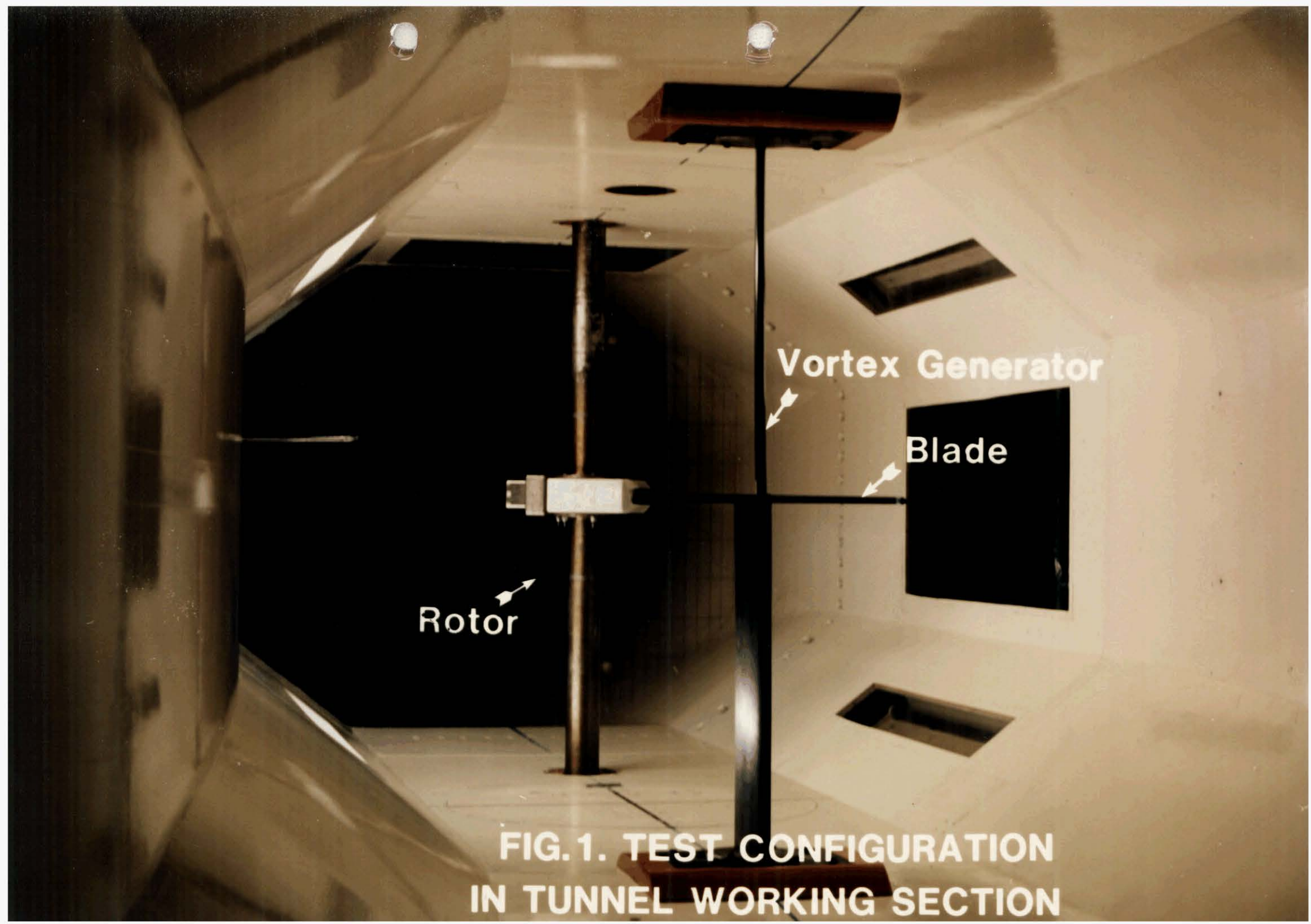

FIG. 1. TEST CONFIGURATION
IN TUNNEL WORKING SECTION

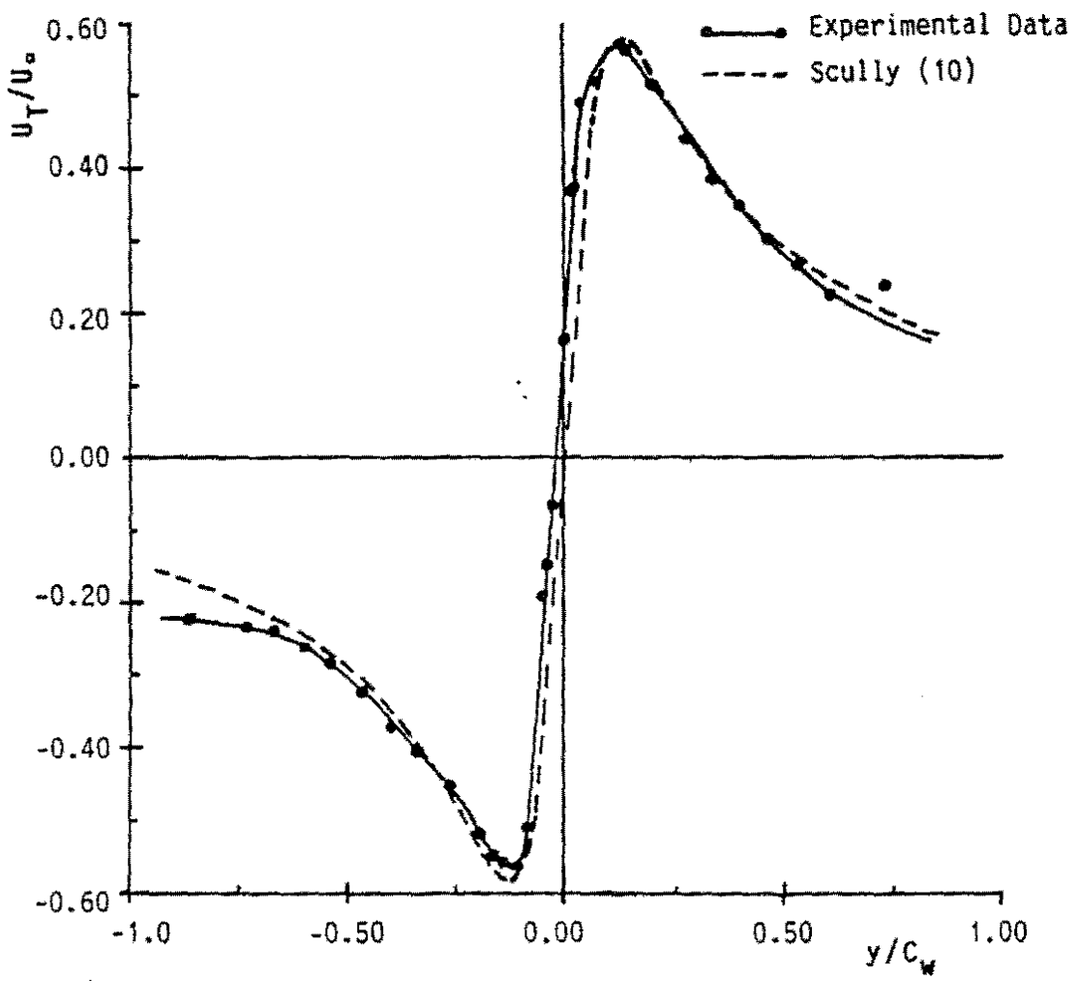

FIG. 3. Distribution of non-dimensional tangential velocity across the vortex core, $\delta=25^{\circ}$, $\Gamma/U_T C_w=0.96$.

LEGEND			
δ^o	$\Gamma(m^2/s)$	$\Gamma/U_T C_w$	d_v/C_w
5	1.10	0.16	0.340
10	2.20	0.32	0.280
15	3.40	0.49	0.270
20	5.10	0.73	0.260
25	6.70	0.96	0.260

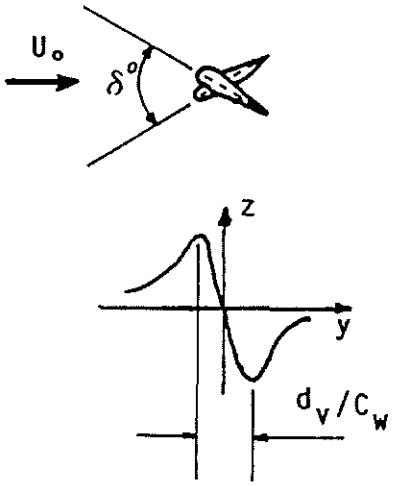

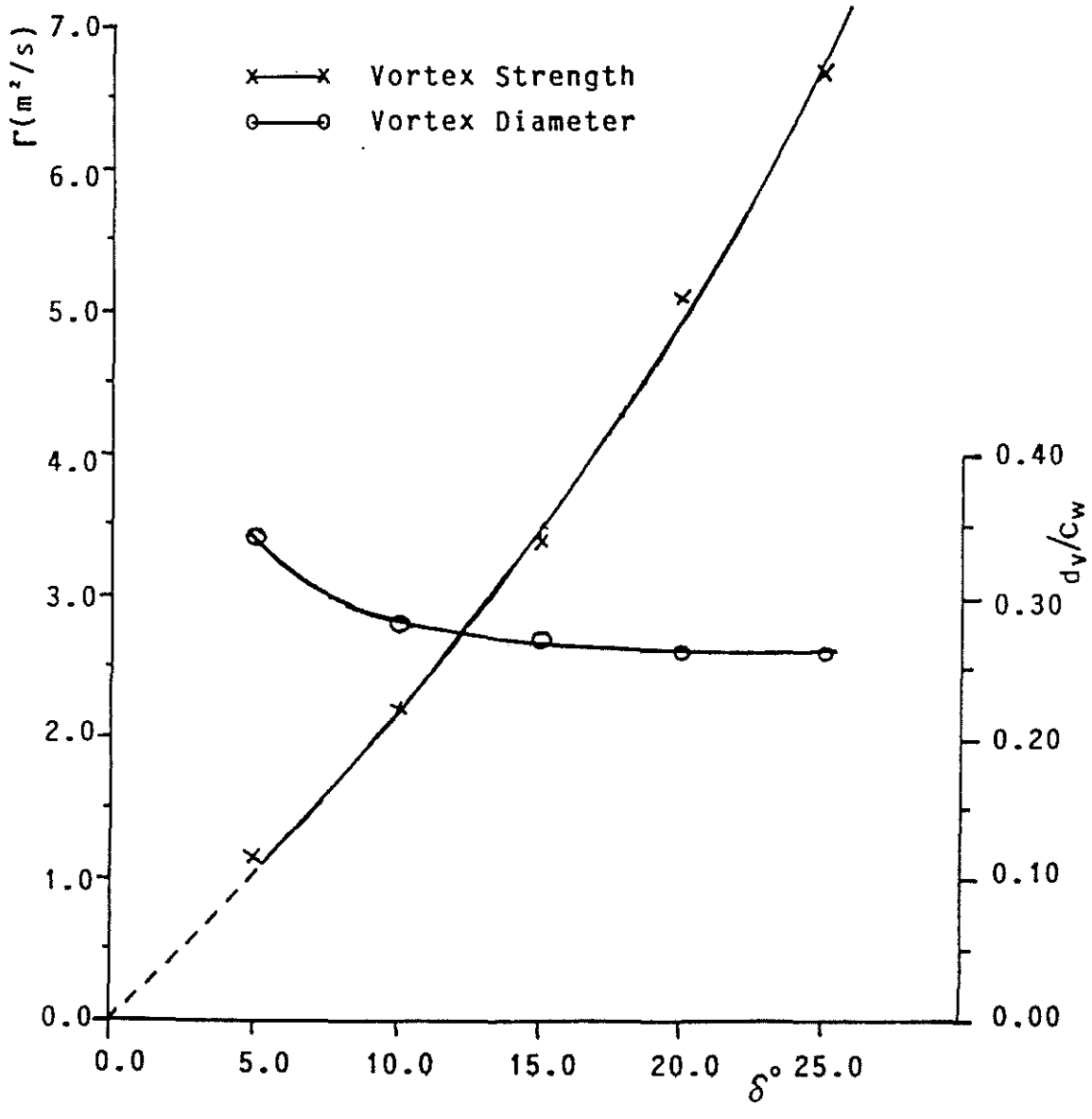

FIG. 4. Variation of vortex strength and core diameter with differential angle-of-incidence of vortex generator.

LEGEND					
SYMBOL	TRANS. NO.	CHORDWISE POS.	SYMBOL	TRANS. NO.	CHORDWISE POS.
▲	1	0.950	○	7	0.125
▼	2	0.860	✱	8	0.100
⊕	3	0.760	△	9	0.075
⧗	4	0.550	▽	10	0.050
□	5	0.350	+	11	0.015
◇	6	0.200			

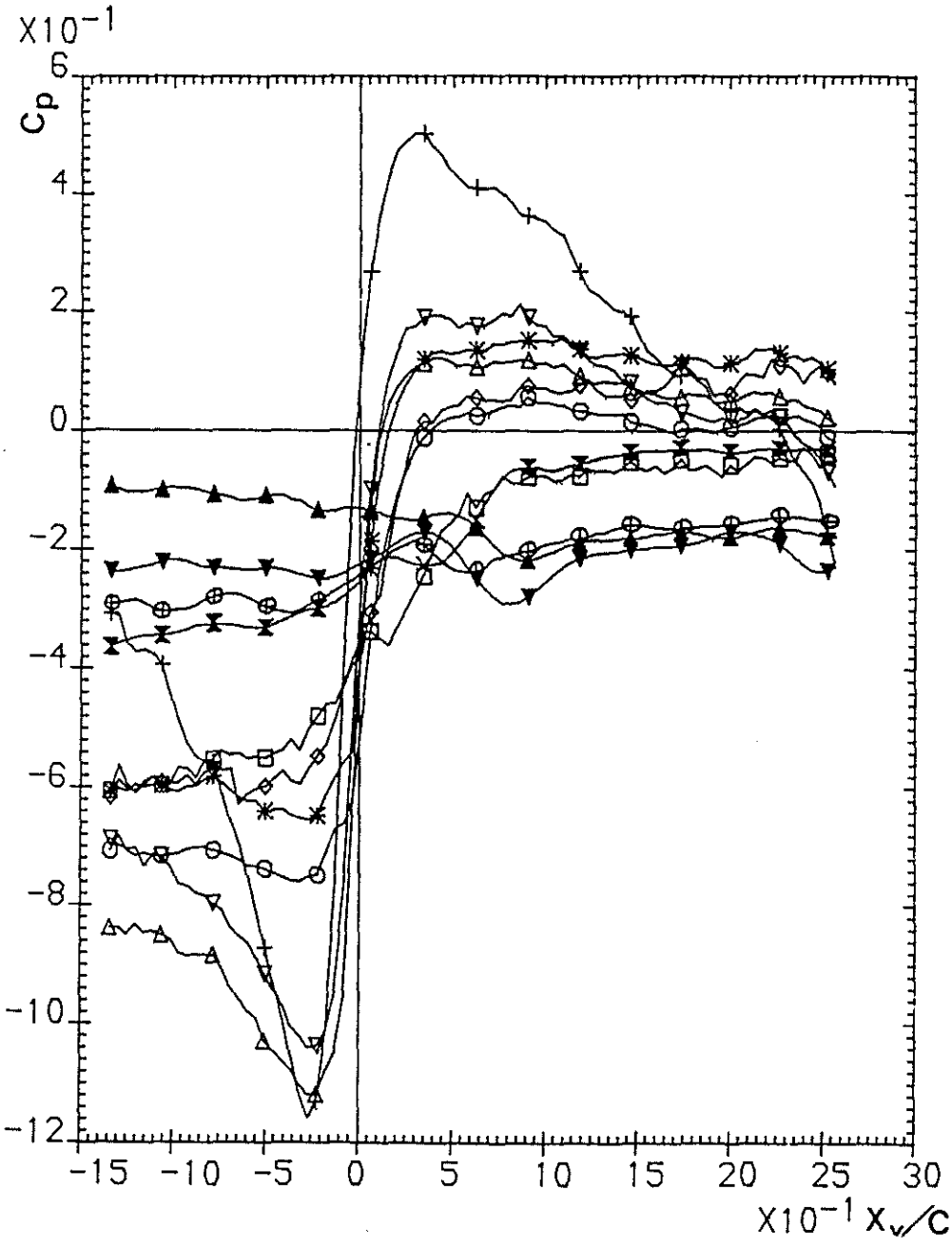

FIG. 5. Vortex induced upper surface (vortex side) pressure variations as a function of vortex chordal position, M_L=0.175, δ=25°, Yv/c=0.20, r/R=0.95 .

LEGEND :					
SYMBOL	TRANS. NO.	CHORDWISE POS.	SYMBOL	TRANS. NO.	CHORDWISE POS.
▲	1	0.950	○	7	0.125
▼	2	0.860	✱	8	0.100
⊕	3	0.760	△	9	0.075
×	4	0.550	▽	10	0.050
□	5	0.350	+	11	0.015
◇	6	0.200			

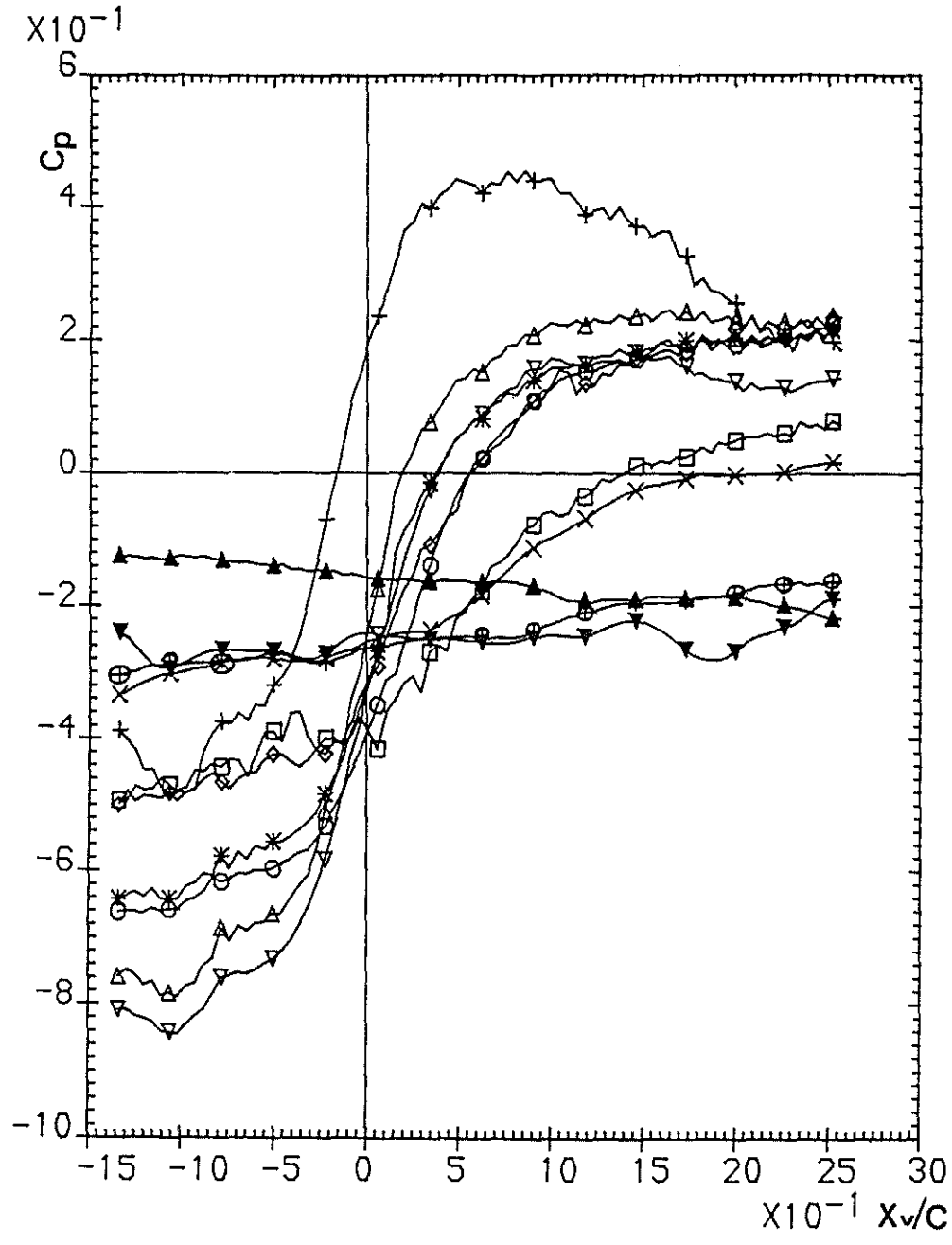

FIG. 6. Vortex induced upper surface (vortex side) pressure variations as a function of vortex chordal position, M_L=0.175, δ=25°, Yv/c=0.60, r/R=0.95 .

LEGEND	
SYMBOL	Yv/c
△	0.00
▽	0.20
+	0.40
×	0.60
□	0.80

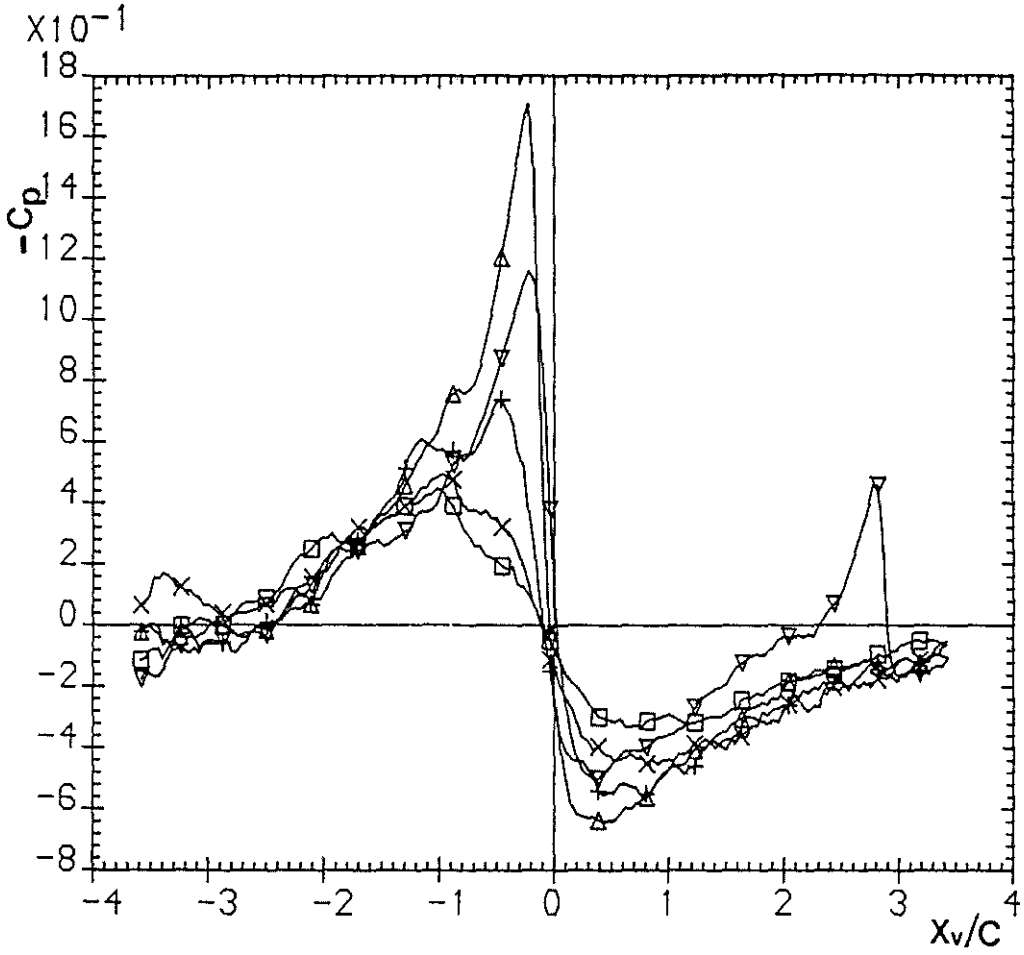

FIG. 7. The effect of rotor blade-tip vortex seperation upon the leading edge pressure variation, M_L=0.175, δ=25°, x/c=0.050, r/R=0.95 .

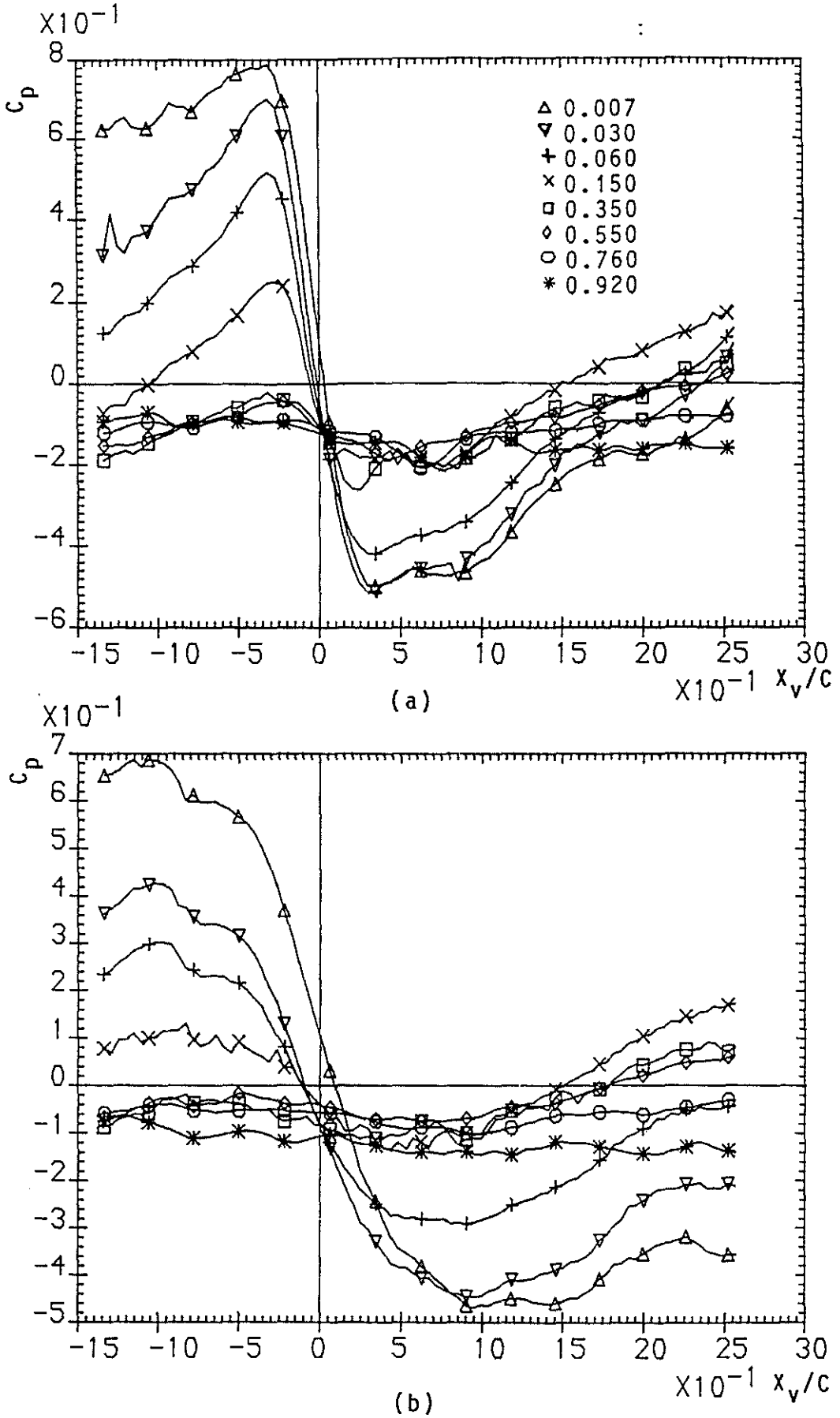

FIG. 8. Vortex induced lower surface pressure variations as a fuction of vortex chordal position,
(a) M_L=0.175, δ=25°, Yv/c=0.20, r/R=0.95
(b) M_L=0.175, δ=25°, Yv/c=0.60, r/R=0.95 .

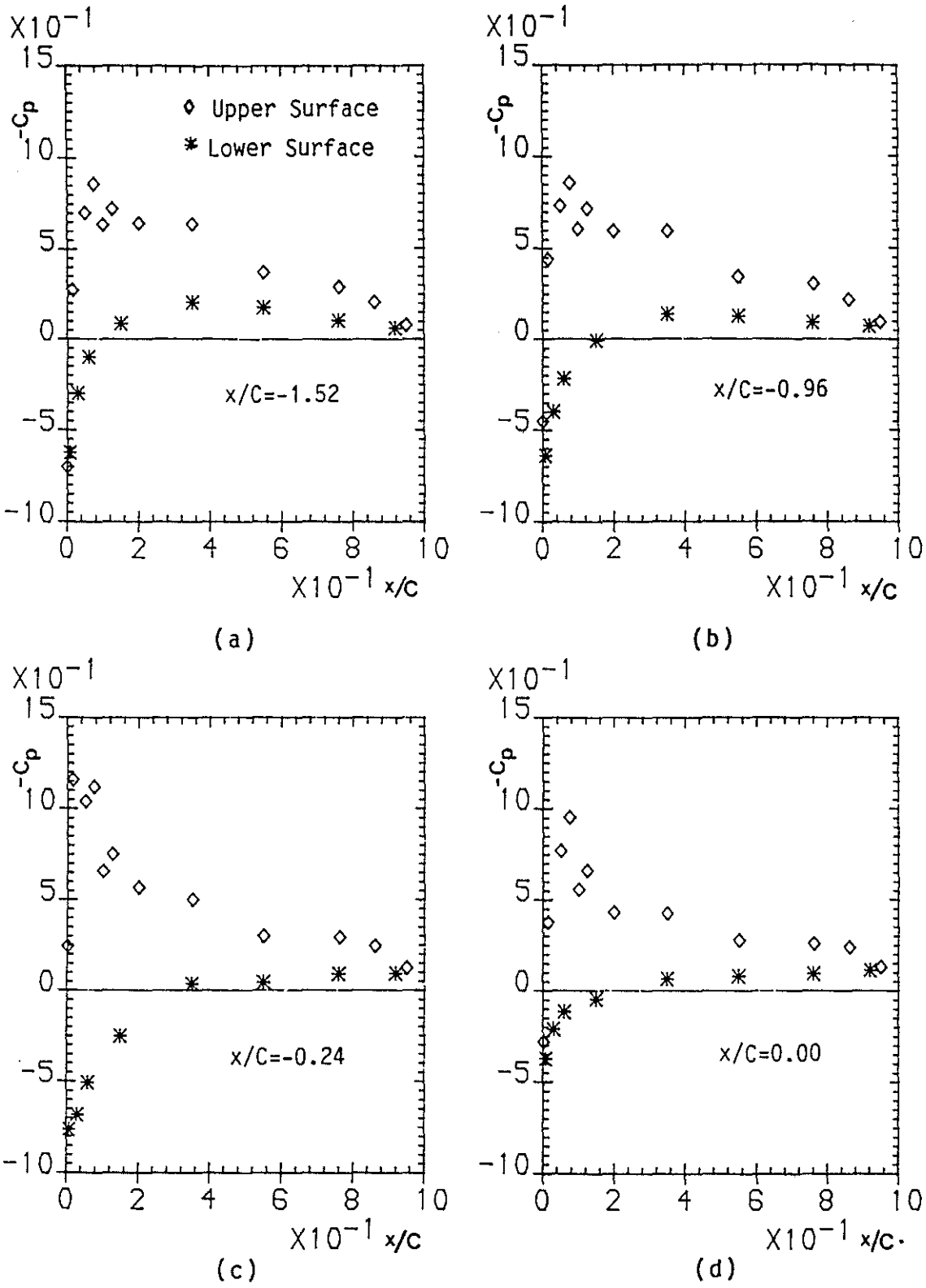

FIG. 9. Chordwise pressure distrbution as a function of vortex chordal position, M_L=0.175, δ=25°, Yv/c=0.20, r/R=0.95 .

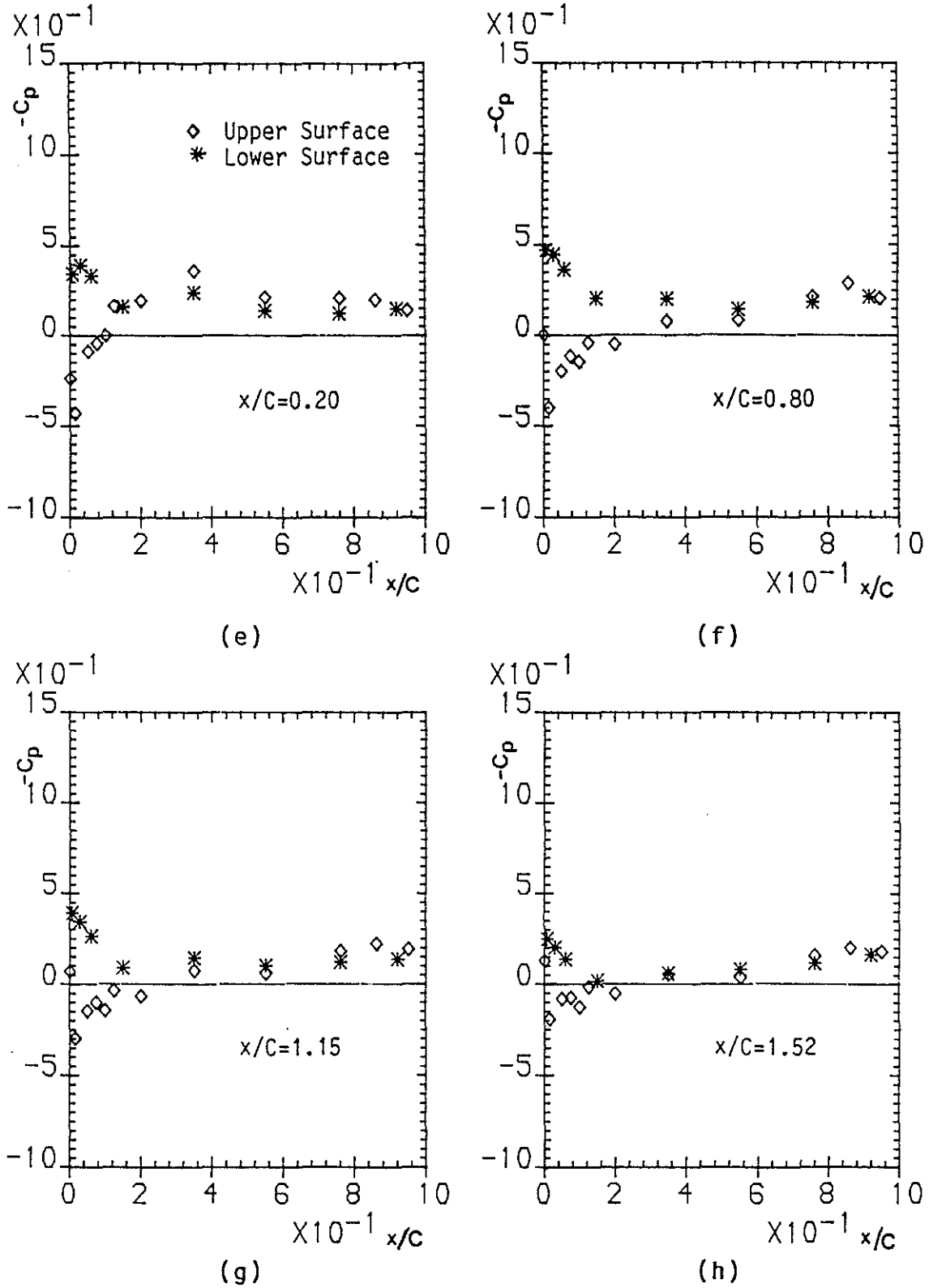

FIG. 9. (Continued)

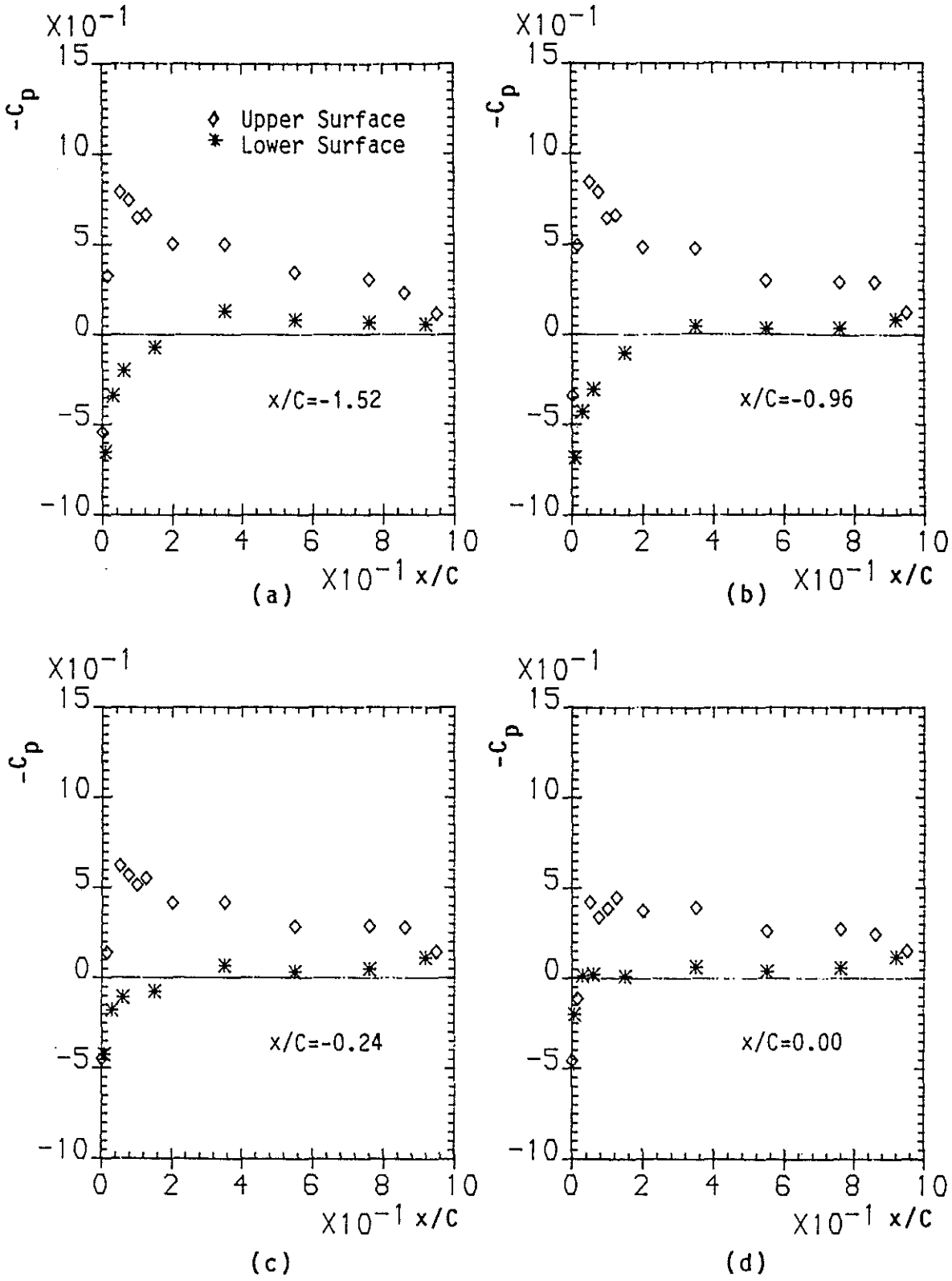

FIG. 10. Chordwise pressure distribution as a function of vortex chordal position, M_L=0.175, δ=25°, Yv/c=0.60, r/R=0.95 .

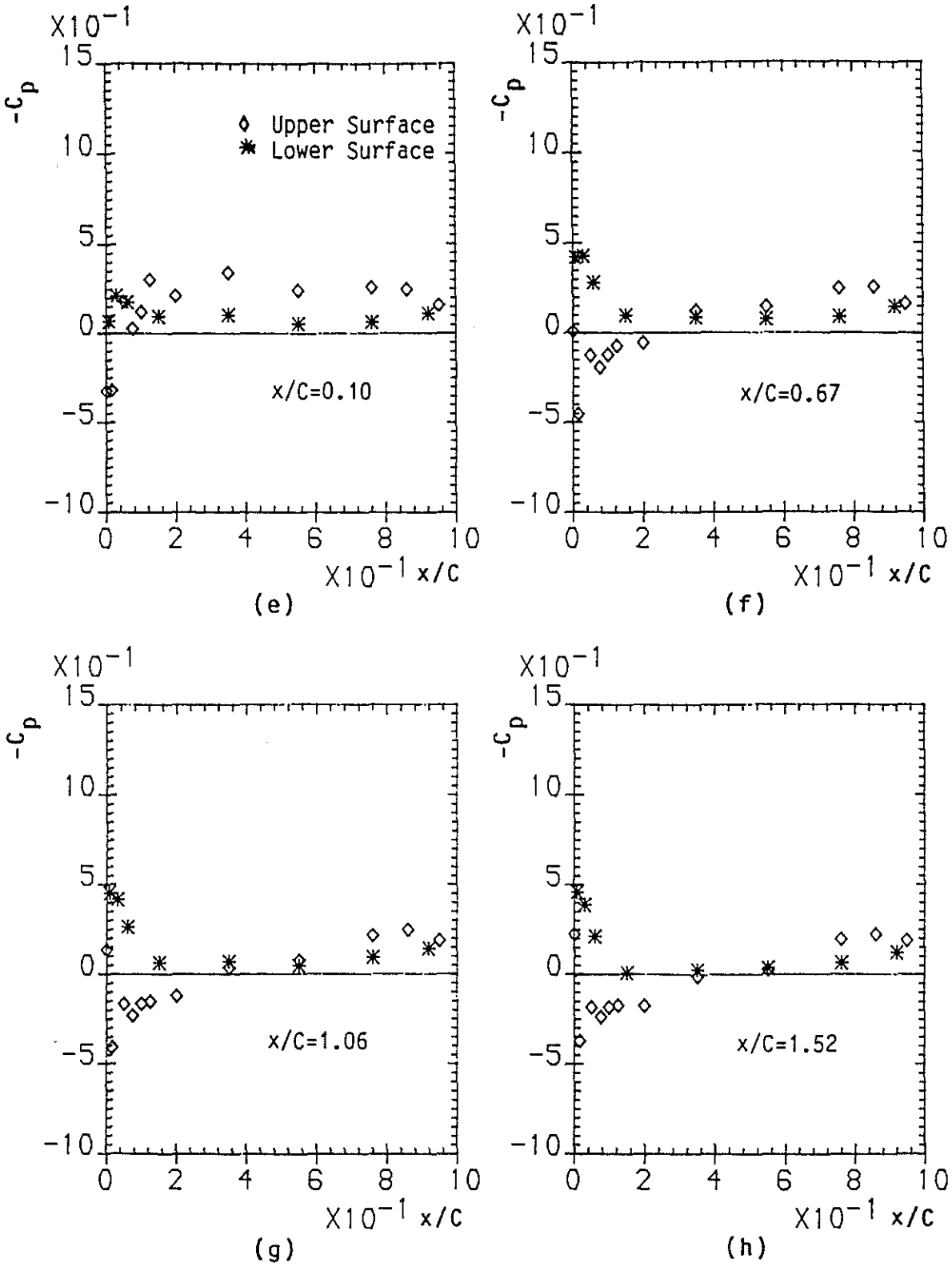

FIG. 10. (Continued)

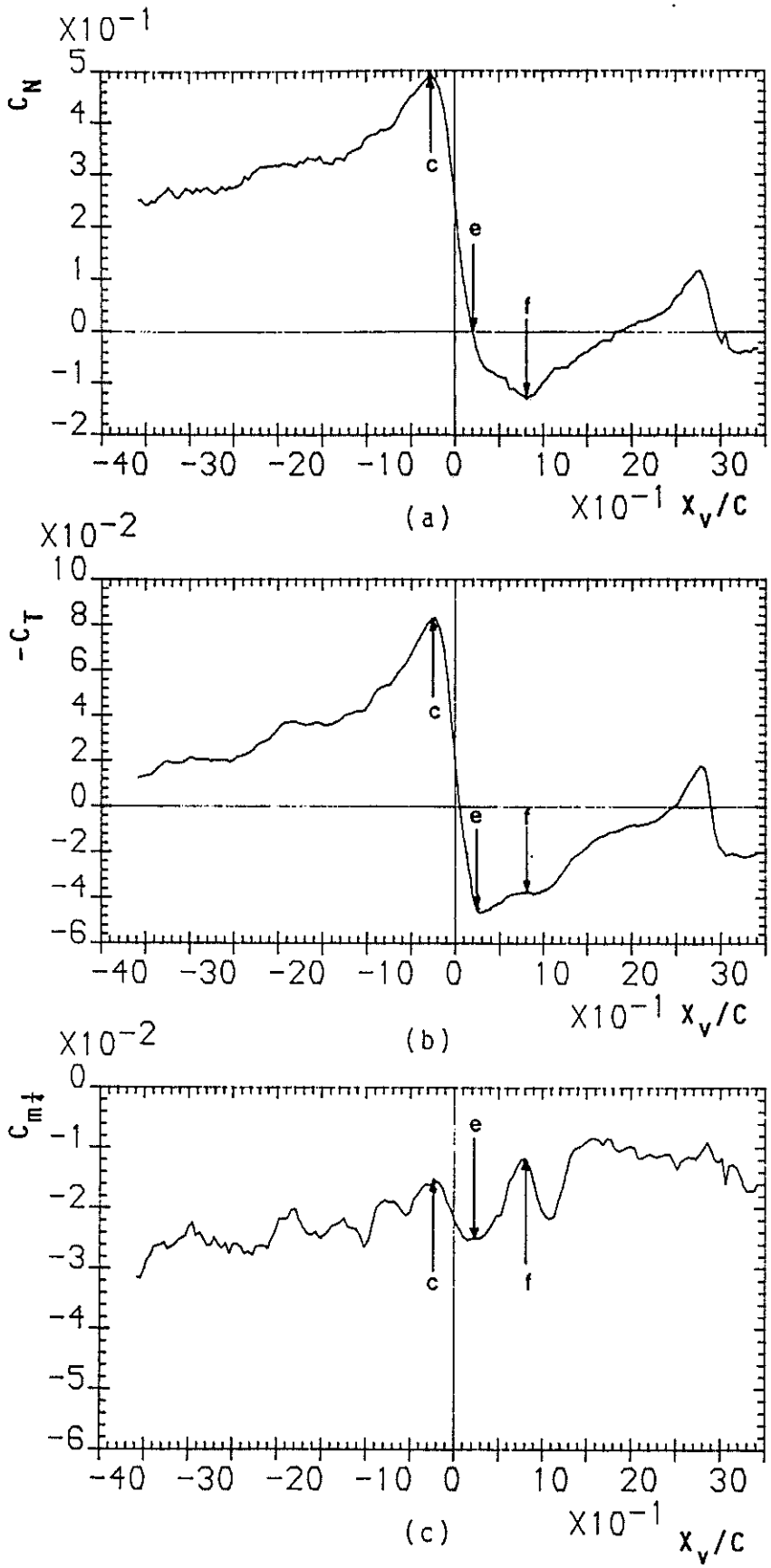

FIG. 11. (a) Normal force, (b) Pressure drag, and (c) ¼-chord Pitching moment coefficient variations as a function of vortex chordal position, M_L=0.175, δ=25°, Yv/C=0.20, r/R=0.95 .

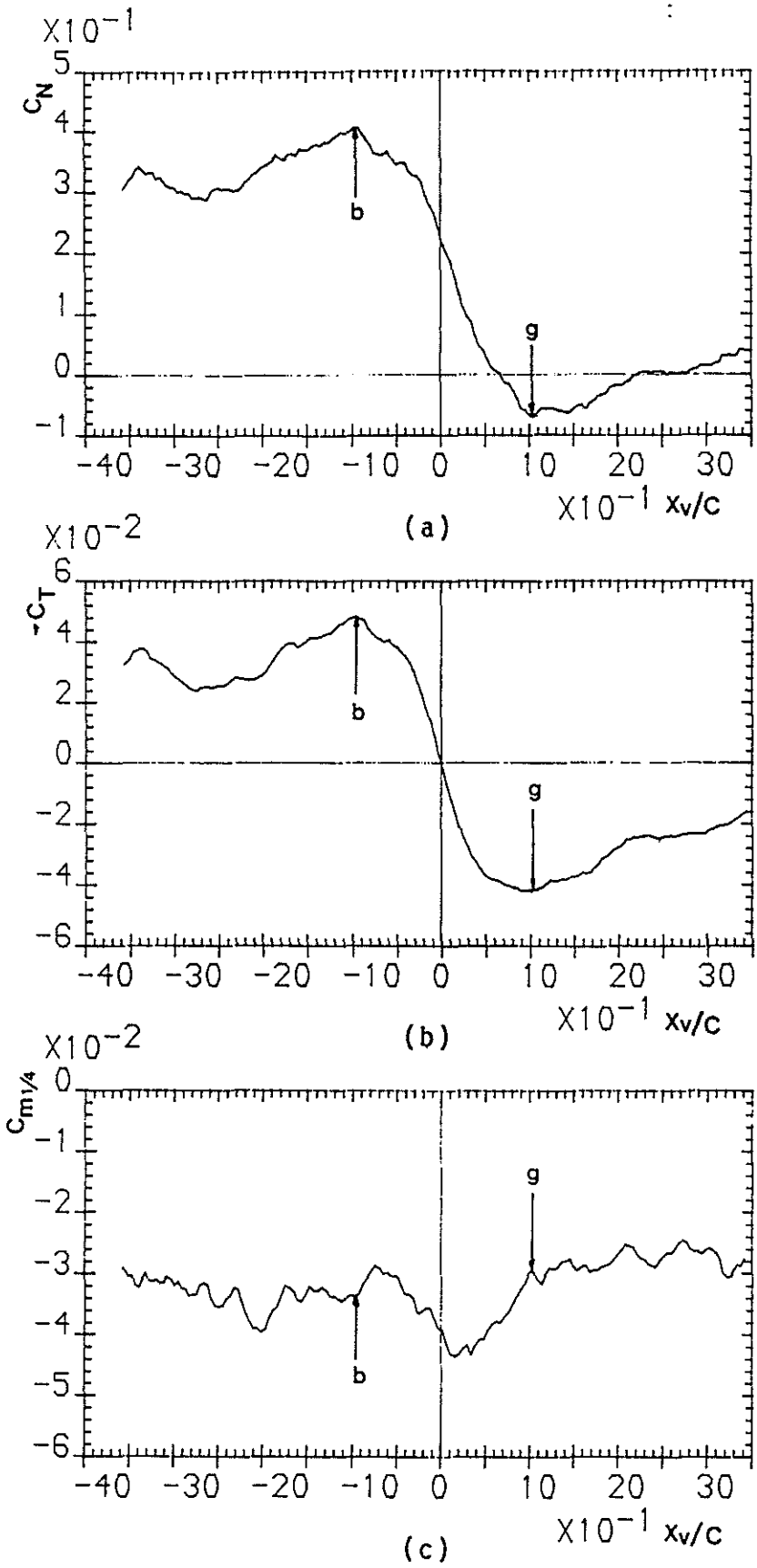

FIG. 12. (a) Normal force, (b) Pressure drag, and (c) $\frac{1}{4}$-chord Pitching moment coefficient variations as a function of vortex chordal position, M_L=0.175, δ=25°, Yv/C=0.60, r/R=0.95 .

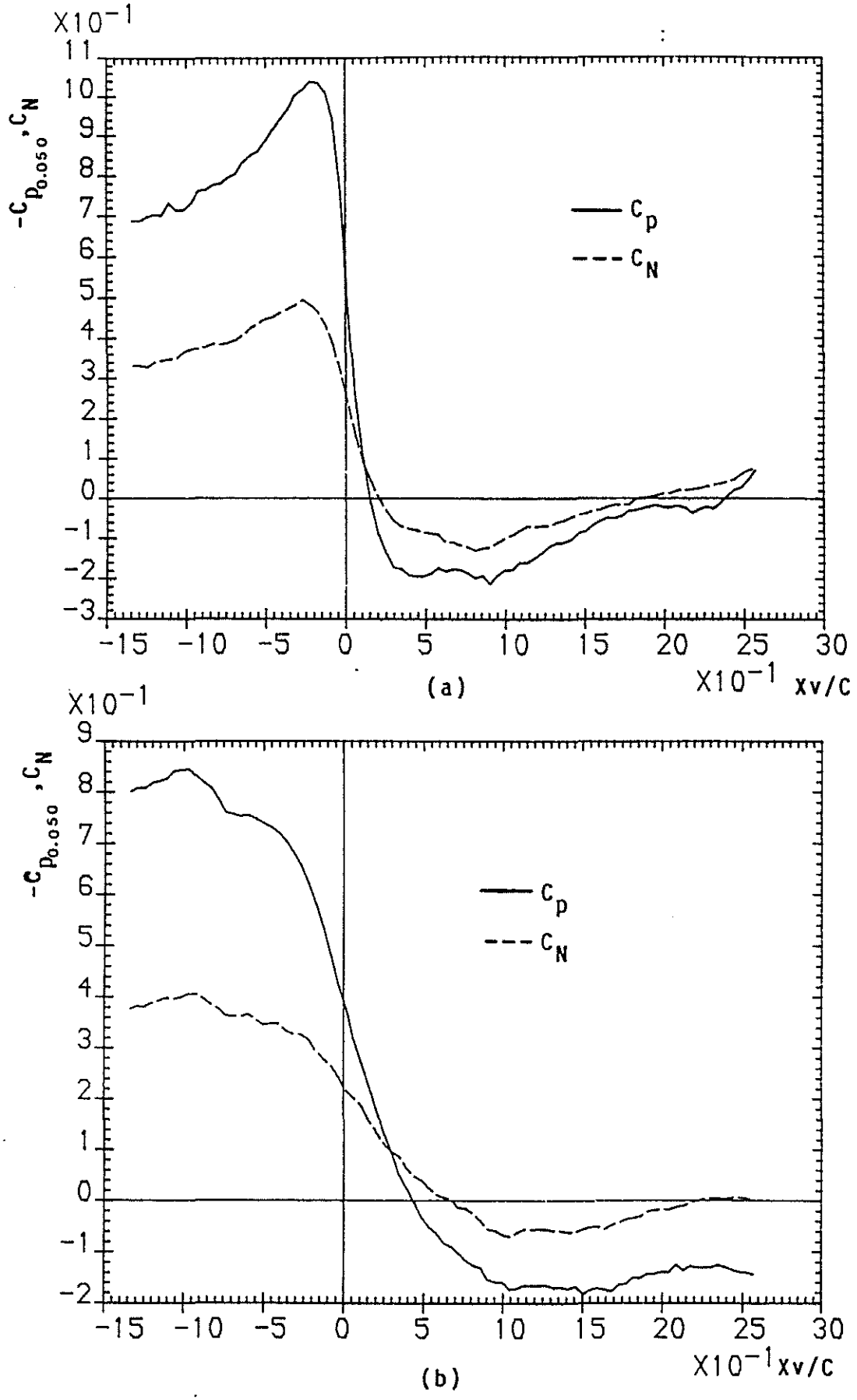

FIG. 13. Plots of Normal force and Leading Edge pressure coefficient variations as a function of vortex chordal distance.
(a) x/C=0.050, δ=25°, Yv/C=0.20, r/R=0.95 .
(b) x/C=0.050, δ=25°, Yv/C=0.60, r/R=0.95 .

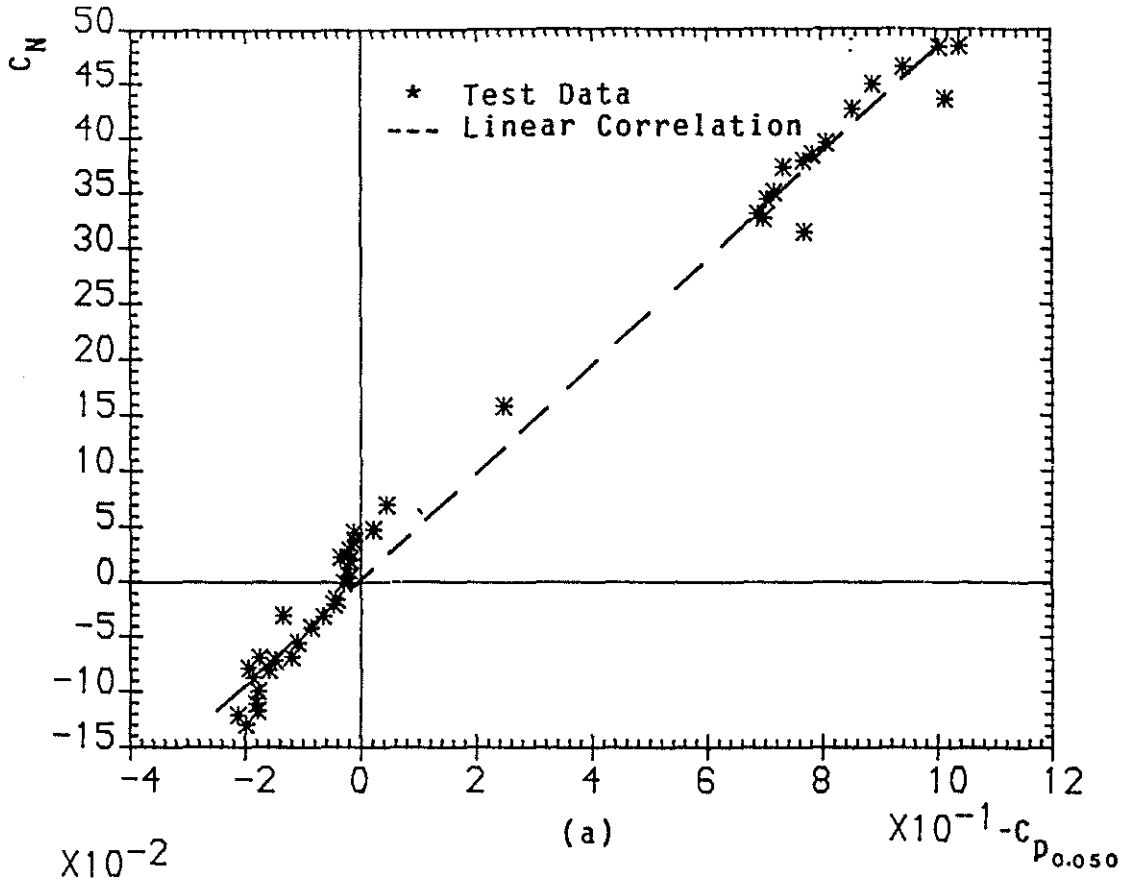

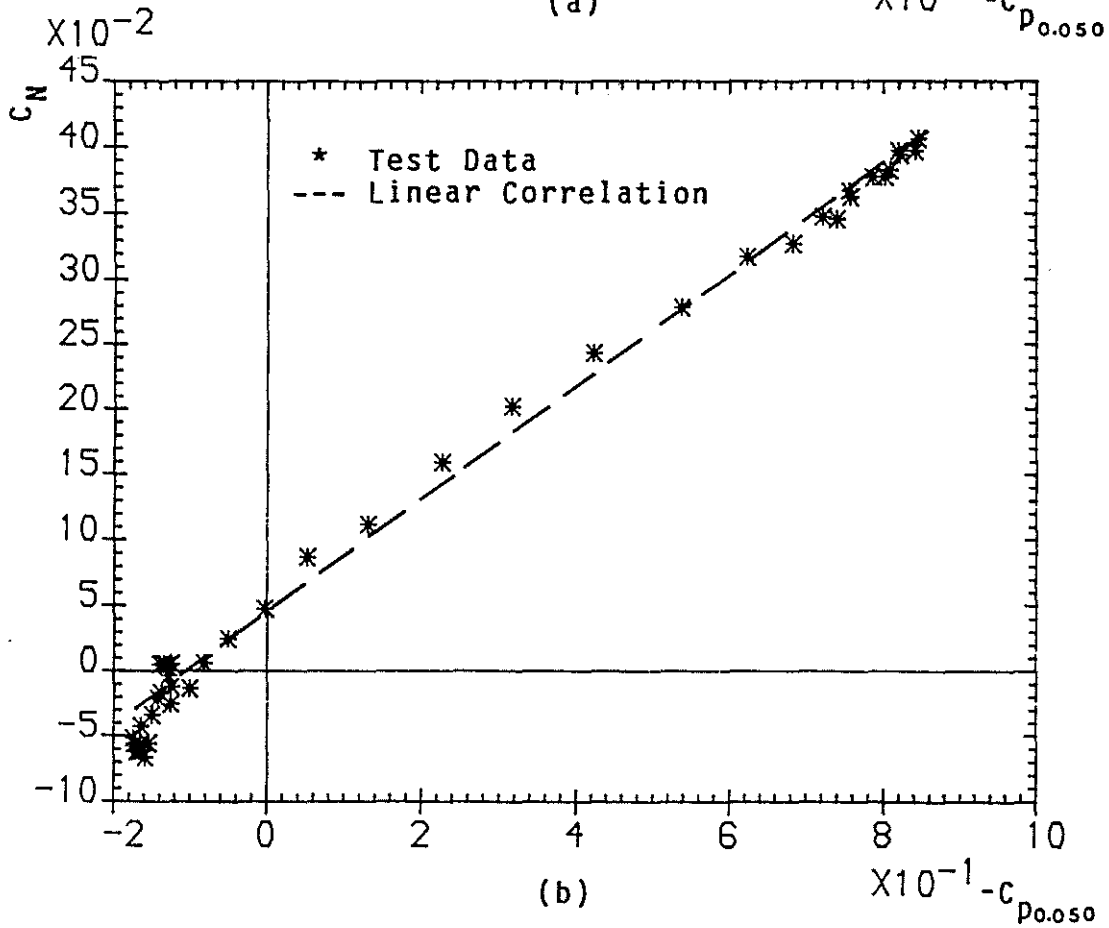

FIG. 14. Correlations between the Normal force and Leading Edge pressure coefficients.
(a) x/C=0.050, =25°, Yv/C=0.20, r/R=0.95 .
(b) x/C=0.050 =25° Yv/C=0.60, r/R=0.95 .

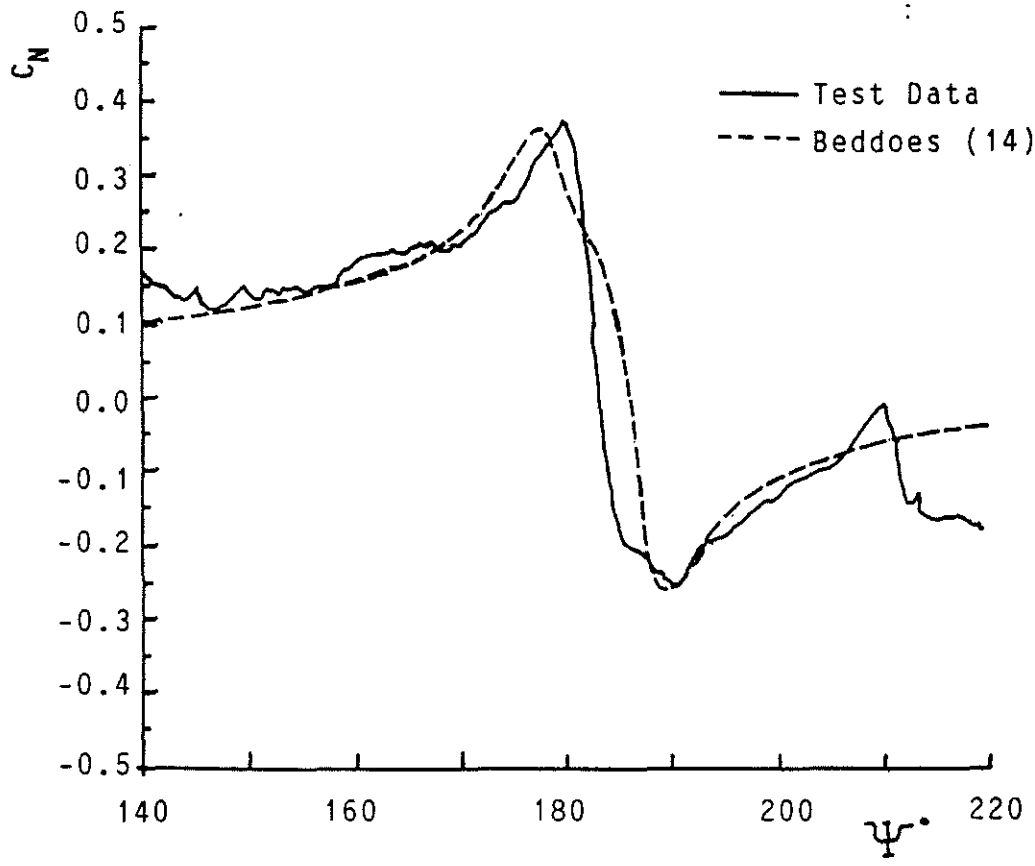

(a)

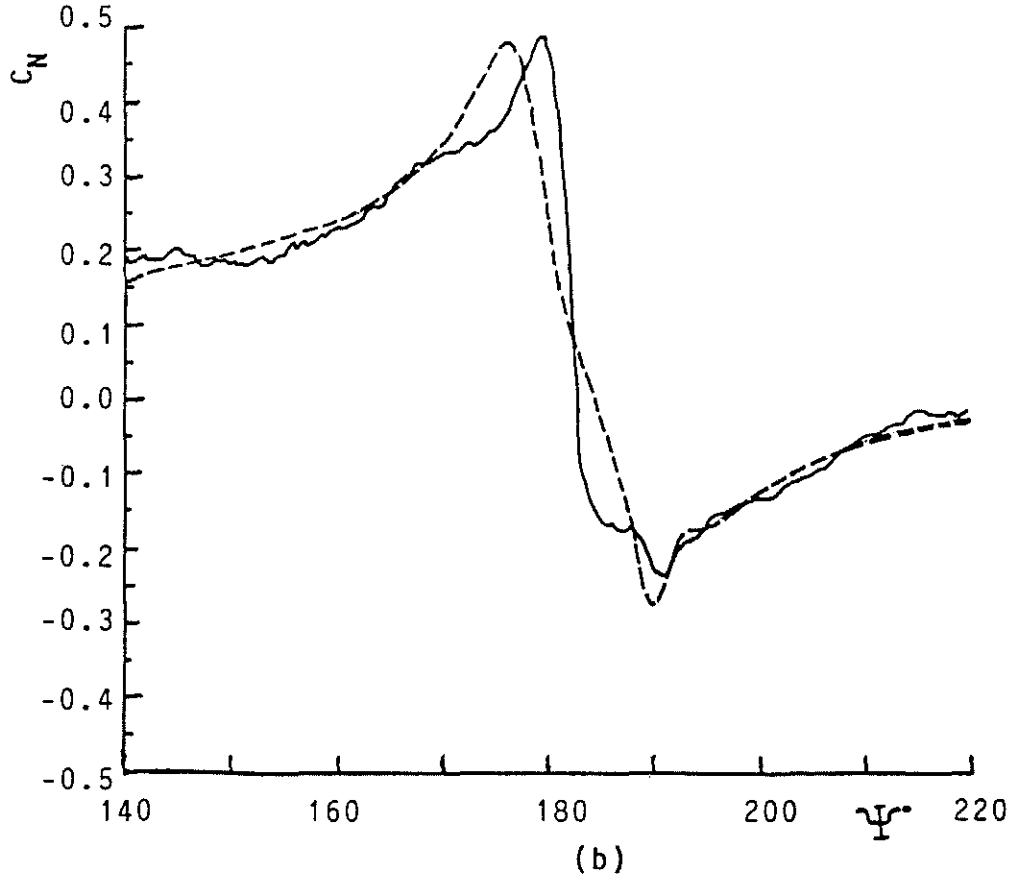

(b)

FIG. 15. Comparison of experimental and theoretical Normal force coefficient variations as a function of blade azimuth, (a) M_L=0.175, δ=25°, Yv/c=0.20, r/R=0.95 (b) M_L=0.175, δ=25°, Yv/c=0.60, r/R=0.95 .